Clim Dyn (2011) 37:1133–1149
DOI 10.1007/s00382-010-0902-3

ENSO regulation of MJO teleconnection

Ja-Yeon Moon · Bin Wang · Kyung-Ja Ha

Received: 27 April 2010 / Accepted: 22 August 2010 / Published online: 5 September 2010

Abstract The extratropical teleconnections associated with Madden–Julian Oscillation (MJO) are shown to have an action center in the North Pacific where the pressure anomalies have opposite polarities between the Phase 3 (convective Indian Ocean) and Phase 7 (convective western Pacific) of the MJO. The teleconnection in the same phase of MJO may induce opposite anomalies over East Asia and North America between El Niño and La Niña years. During MJO Phase 3, a gigantic North Pacific anticyclonic anomaly occurs during La Niña, making coastal northeast Asia warmer/wetter than normal, but the west US colder/drier; whereas during El Niño the anticyclonic anomaly is confined to the central North Pacific, hence the northwest US experiences warmer than normal weather under influence of a downstream cyclonic anomaly. During Phase 7, an extratropical cyclonic anomaly forms over the northwest Pacific during La Niña due to convective enhancement over the Philippine Sea, causing bitter winter monsoon over Japan; whereas during El Niño, the corresponding cyclonic anomaly shifts to the northeast Pacific due to enhanced convection over the equatorial central Pacific, which causes warm and wet conditions along the west coast of US and Canada. Further, the presence of ENSO-induced seasonal anomalies can significantly modify MJO teleconnection, but the aforementioned MJO teleconnection can still be well identified. During Phase 3, the MJO teleconnection pattern over North Pacific will be counterbalanced (enhanced) by El Niño (La Niña)-induced seasonal mean anomalies. During Phase 7, on the other hand, the MJO teleconnection anomalies in the northeastern Pacific will be enhanced during El Niño but reduced during La Niña; thereby the impacts of MJO teleconnection on the North America is expected to be stronger during El Niño than during La Niña.

Keywords MJO teleconnection · ENSO regulation · Intraseasonal variation

J.-Y. Moon · B. Wang
International Pacific Research Center,
School of Ocean and Earth Science Technology,
University of Hawaii at Mânoa, Honolulu, HI, USA

K.-J. Ha (✉)
Division of Earth Environmental System,
Pusan National University, Busan, Korea
e-mail: kjha@pusan.ac.kr

1 Introduction

Through changing tropical diabatic heating, the Madden–Julian Oscillation (MJO) may influence extratropical circulation by teleconnection (Lau and Philips 1986; Knutson and Weickmann 1987; Ferranti et al. 1990; Higgins and Mo 1997; Matthews et al. 2004). In association with eastward propagation of the MJO convective anomaly is a Rossby-Kelvin wave structure in the upper-troposphere with a pair of anticyclones to the west of and alongside the convection/upward motion and a pair of cyclones to the east (Murakami 1988; Rui and Wang 1990). When enhanced convection is observed over the Indian Ocean and the western Pacific, a chain of cyclonic and anticyclonic disturbances develops downstream of the upper-level convective outflow, mainly in the exit region of the East Asian Jet (Hsu 1996; Kim et al. 2006). In the lower-level, a pair of cyclonic anomalies is nearly 180° out of phase with the corresponding upper-level anticyclones, which dissipate after reaching the central Pacific, although the upper tropospheric anomalies continue to traverse the Western Hemisphere (Lorenc 1984; Knutson et al. 1986; Rui and Wang 1990; Cassou 2008). As a part of a teleconnection

pattern, Murakami (1988) noted strong 30–60 day meridional wind anomalies surging from cold mid-latitudes. Higgins et al. (2000) showed coherent relationships between eastward evolving tropical convection from the western to central Pacific, with extreme precipitation over the Pacific Northwest to the west coast of the United States on intraseasonal timescales. Lagged relationship between the MJO and mid-latitude low-frequency wavetrain over North Atlantic-Europe regimes has been found by Cassou (2008); suggesting that the MJO can even affect phases of the North Atlantic Oscillation.

In the present study, *MJO teleconnection* is considered as the upper-level succession of cyclonic and anticyclonic disturbances downstream of the MJO convective outflow in reference to the counterpart lower-level circulation anomalies.

In the context of interannual variations, El Niño-Southern Oscillation (ENSO) is the most energetic and predictable mode of the global climate system, and its relation with the MJO has been extensively studied (Lau and Chan 1988; Lau and Shen 1988; Weickmann 1991; Takayabu et al. 1999; Kessler and Kleeman 2000; Bergman et al. 2001; Zhang and Gottschalck 2002; Teng and Wang 2003; Lau 2005; Hendon et al. 2007; Yun et al. 2008, 2009; among many others). Some studies have suggested that the overall amplitude of the MJO activity is not appreciably affected by the presence of El Niño or La Niña (Slingo et al. 1999; Kessler 2001). However, during mature phases of El Niño events the MJO activity markedly shifts eastward into the central Pacific, expanding the longitudinal domain of the MJO convective activity (Fink and Speth 1997; Hendon et al. 1999; Kessler 2001). Lagged relationships were also recently discovered between the MJO activity in spring and the state of El Niño in subsequent autumn/winter seasons, suggesting that the warming in the eastern Pacific could be initiated by the intraseasonal oscillation via eastward propagation of the warm pool and the development of surface westerly anomalies (Hendon et al. 2007; Pohl and Matthews 2007).

Several studies have discussed the impact of ENSO on the extratropical intraseasonal variability during the boreal winter (Namias 1986; Chen and Van den Dool 1997; Tam and Lau 2005). The ENSO may influence intraseasonal activity in the extratropics through its effect on the basic state stability. On the other hand, a modeling study of Compo et al. (2001) suggested that tropical forcing is an important factor in determining intraseasonal variability in the extratropics, as they found that both the tropical precipitation and extratropical circulation on intraseasonal time scales are strongly affected by ENSO. Tam and Lau (2005) have shown that the amplitude of intraseasonal variability over the North Pacific was enhanced in cold ENSO events as compared to warm events, suggesting that ENSO can influence the North Pacific intraseasonal activity through its effects on the evolution of convective anomalies in the tropical western Pacific.

Despite the studies reviewed above, the relationship between the and ENSO has not been clearly quantified; hence the ENSO regulation on the MJO teleconnection is still not fully understood.

The present study aims to better detect and predict the ENSO impacts on MJO teleconnection. We focus on the tropical-extratropical teleconnection when MJO convection is active over the Indian and western Pacific Oceans and understanding of the cause of interannual variability of the MJO and associated extratropical circulation anomalies (MJO teleconnection). We shall show that the MJO teleconnection have distinct interannual characters due to ENSO-induced basic state changes. In Sect. 2, the data and statistical method used in this study are described. The interannual variation of the tropical-extratropical intraseasonal variability especially those associated with ENSO is documented in Sect. 3. Since the MJO propagates along the equator, the MJO teleconnection is phase-dependent. Hence, the influence of ENSO on the MJO teleconnection at two major phases is contrasted in details in Sect. 4. Conclusion and discussion are given in Sect. 5.

2 Data and methodology

Since the MJO and ENSO both mature in boreal winter, the present study focuses on boreal winter from December through February (DJF). The data used include National Centers for Environmental Prediction-National Center for Atmospheric Research (NCEP-NCAR) reanalysis (Kalnay et al. 1996) daily mean horizontal wind, streamfunction, temperature, precipitable water, Advanced Very High Resolution Radiometer (AVHRR) daily mean outgoing longwave radiation (OLR), and National Oceanic Atmospheric Administration (NOAA) monthly mean Extended Reconstruction Sea Surface Temperature (ERSST) V3 data from 1979 to 2008. Based on the well-established Niño3.4 (Trenberth 1997) index, the boreal winters of 1982, 1986, 1987, 1991, 1994, 1997, 2002, 2004 are selected as El Niño years and 1984, 1988, 1995, 1998, 1999, 2000, 2007 as La Niña years.

The time mean and first three harmonics of the annual cycle were first removed from the local time series of variables for the 1979–2008 periods. The interannual variability associated with ENSO were then removed by using the time series of the first EOF of Indo-Pacific SSTs (Drosdowsky and Chambers 2001) and a 120-day mean during the previous 120 days was also subtracted. The MJO index defined by Wheeler and Hendon (2004, hereafter WH04) was used to identify phases of MJO life cycle.

The principal components of the first two leading EOFs of the combined daily tropical (averaged between 15°S and 15°N) zonal winds at 850 hPa (U850) and 200 hPa (U200) and OLR anomalies are plotted in the phase space to trace MJO life cycle (Fig. 7 of WH04). The numbered phases indicate locations of enhanced convection in MJO life cycle: Phase 2 and 3 at Indian Ocean, Phase 4 and 5 at Maritime Continent, Phase 6 and 7 at western Pacific, and Phase 8 and 1 at Western Hemisphere and Africa. A composite method was used to derive tropical and extratropical teleconnection map with reference to these phases. The composite maps were made by average of intraseasonal anomaly fields occurring during each phase with amplitude exceeding one standard deviation of 1979–2008 time series of combined EOF1 and EOF2. We selected two representative MJO phases (Phase 3 and 7) to carefully compare the horizontal structures of MJO and MJO teleconnection between El Niño and La Niña years. A Student's *t* test was used to assess the statistical significance of the composite intraseasonal anomalies of the selected phase during ENSO.

3 Interannual variation of tropical-extratropical intraseasonal variance

3.1 Mean flow changes associated with the ENSO

The mean background fields are important as they affect the organization, intensification, and propagation of the intraseasonal oscillation and teleconnection (Kemball-Cook et al. 2002). To facilitate our discussion of joint tropical-extratropical intraseasonal variations, the changes in the planetary scale mean flow associated with ENSO is first briefly reviewed. Figure 1 shows that the climatological SST warm pool, intensive convective activity, upper-level westerly jet are displaced/changed differently during opposite phases of the ENSO cycle. During La Niña, the edge of the warm pool (SST $\geq$ 28°C and T850 $\geq$ 290 K) extends poleward over the Philippine Sea but retreats westward over the equatorial central Pacific; the corresponding intensive convective activity (OLR $\leq$ 225 Wm^{-2}) is markedly enhanced over the vicinity of Philippines and SPCZ (South Pacific Convergence Zone) with a drastic westward retreat over the equatorial central Pacific; the upper-level subtropical jet stream (U300 $\geq$ 25 ms^{-1}), which acts as a waveguide, over the Africa—Pacific—North America is positioned further north with the strength in the subtropical central Pacific much reduced. In El Niño, the warm pool and strong convective area extends more to the equatorial central Pacific and the jet stream is located to the south, enhanced over the subtropical central Pacific and southern US.

The ENSO-induced seasonal mean anomalies of SST, OLR, 850 hPa temperature (T850), 300 hPa zonal wind (U300), streamfunction (SF300), 850 hPa streamfunction (SF850) in Fig. 1 show opposite polarities between El Niño and La Niña. The most prominent feature in both the temperature (SST and T850) and convection (OLR) over the tropics is the latitudinal expansion of the enhanced anomalies and warm water during La Niña, which occurs mainly over the eastern Indian and western Pacific Oceans. On the other hand, the positive SST and negative OLR anomaly centers are located at the equatorial central Pacific in El Niño years. In the extratropics, dipole anomaly over the North Pacific/North America in the T850 field is dominant in both El Niño and La Niña years, in which the cold/warm anomaly prevails in El Niño and the opposite in La Niña. Corresponding to these changes, the upper-level wind have the largest circulation change from the central-eastern tropical Pacific through North America and South Asian sectors. In La Niña, the anticyclonic flows (SF300) over the eastern North Pacific, South Asia, and southern US are enhanced. In the low-level (SF850), the barotropic anticyclonic flow over the North Pacific is intensified. Reversed anomalies tend to occur during El Niño.

3.2 Interannual variation of intraseasonal variance

Figure 2 displays the winter mean intraseasonal variability (ISV, contour) and its interannual variation (shading), as measured by the standard deviation of the intraseasonal variance during the period of 1979–2008. The most pronounced interannual variation of the ISV of OLR is found along the boundaries of the seasonal mean ISV center (Fig. 2a); namely, at the equatorial central-eastern Pacific and along the off-equatorial latitude bands between 10° and 25° over the Indian Ocean and western-central Pacific in both hemispheres. This indicates that the interannual variability of the convection associated with the MJO has large fluctuation in the meridional direction over the warm pool region, but in the zonal direction over the equatorial central-eastern Pacific.

The large ISV of the streamfunction is confined to the north of 20°N in the NH (Fig. 2b, c). The seasonal mean ISVs of the 850 hPa streamfunction (SF850) and 300 hPa streamfunction (SF300) show consistent structures with maximum centers located over the North Pacific and North Atlantic (around 40°N) where the predominant atmospheric low-frequency teleconnection occurs (Wallace and Gutzler 1981). At the low-level, the interannual variation of ISV has almost the same structures as that of the seasonal mean ISV (Fig. 2b). At the upper-level, however, the large interannual variation occurs along two latitudinal bands, one in the subtropics (20°–40°N) and the other at high latitude (50°–70°N; Fig. 2c). The variability over the

subtropical band is related to the variability of OLR ISV in the off-equatorial region, since a standard deviation of the SF300 larger than 1.5 is located to the north of the corresponding OLR ISV regions in the NH. At the high latitude band, the maximum variability is centered over the Bering Sea, Iceland and Scandinavia, which are located at the northern edge of the core regions of the mean ISV.

3.3 Intraseasonal variance associated with ENSO

Figure 3 compares the composite anomalies of the intraseasonal variability of the OLR and SF850 during El Niño and La Niña years. The most distinguishable feature between El Niño and La Niña is the latitudinal and longitudinal movements of the enhanced intraseasonal convection centers. The ISV intensifies at the equatorial central Pacific during El Niño; in contrast, the ISV intensifies over the Bay of Bengal—South China Sea—Philippine Sea and the subtropical central Pacific in both hemispheres during La Niña years (Fig. 3a, b). It is noteworthy that the ISV of OLR enhances over the tropics, close to the equator in El Niño, while it intensifies close to or at the subtropics in both hemisphere, especially, at the northern edge of the seasonal mean ISV maximum during La Niña. This also indicates that the distribution of the interannual variation of MJO (Fig. 2a) is largely explained by ENSO effect, in which the off-equatorial (equatorial) interannual variation of ISV is explained by La Niña (El Niño).

Figure 3c, d show that the composite anomalous ISV patterns in the SF850 between El Niño and La Niña tend to be opposite. At 850 hPa, the ISV anomalies show southeastward wave train from the western North Pacific to the Gulf of Mexico in both El Niño and La Niña with the opposite polarities. The same is true over the Southeast Asia and north Atlantic. The large variability regions during both El Niño and La Niña years resemble those of interannual variation of ISV in Fig. 2b and c, suggesting that the ENSO has dominate contribution to the interannual variations of the extratropical ISV in rotational circulation (streamfunciton).

4 ENSO regulation of the MJO teleconnection

The general characteristics of the interannual variation of the joint tropical-extratropical intraseasonal variability were described in the previous section. In this section how the ENSO regulates the MJO teleconnection will be investigated further. Since the MJO is characterized by equatorial eastward propagation of convective anomaly coupled with a pair of large-scale anomalous Walker cells (Madden and Julien 1971, 1994), the MJO teleconnection is necessarily MJO phase-dependent. Normally, the MJO convective anomalies develop and mature over the Indian Ocean, often weakening over the Maritime Continent, and redevelop over the western Pacific Ocean (Wang and Rui 1990). Over the warm waters of the Indian and western Pacific, the MJO exhibits large-scale convection anomalies, which interact strongly with the tropospheric circulation and surface fluxes of mass, heat, and momentum (Waliser et al. 2009). Once the disturbances reach the dateline; thus, over cool equatorial waters, the convection demises and the disturbance is seen only in dynamical fields (Rui and Wang 1990; Hendon and Salby 1994; Matthews 2000; Sperber 2003; Kiladis et al. 2005). In view of this canonical life cycle of MJO, two representative MJO phases are selected; Phase 3 when the maximum convection is located over the Indian Ocean and Phase 7 when the active convection is over the western Pacific. As noted earlier, the composites of all variables are obtained by taking average of the intraseasonal anomaly fields occurring for the days that fall within Phase 3 and Phase 7 during El Niño and La Niña years, respectively.

Fig. 1 Contrasting changes in **a**, **b** SST, **c**, **d** OLR, **e**, **f** 850 hPa ▶ temperature (T850), **g**, **h** 300 hPa zonal wind (U300), **i**, **j** streamfunction (SF300) and **k**, **l** 850 hPa streamfunction (SF850) during El Niño and La Niña years in boreal winter (December–February). Composite 28°C SST contours (outlining the warm pool), 225 W/m^2 OLR contours (outlining intense convective activity), 291 K T850 contours (outlining the warm pool) and 25 m/s U300 contours (outlining strong wind) are plotted using *thick lines*. Composite SST, OLR, T850, U300, SF300 and SF850 anomalies are shown by *thin* contours. Units of SST, OLR, T850, U300, SF300 and SF850 are °C, W/m^2, K, m/s, 10^{-6} m/s and 10^{-6} m/s, respectively

4.1 The MJO teleconnection in ENSO neutral years

Prior to examination of the possible ENSO regulation of MJO teleconnection, it is wise to first briefly examine the structures of phase-dependent MJO teleconnection during neutral years of ENSO cycle (without significant influences from the ENSO). Figure 4 shows the neutral year composite map of MJO teleconnection using OLR, 850 and 300 hPa circulations, and 850 hPa temperature at Phase 3 and 7. At Phase 3, the enhanced MJO convection over the eastern Indian Ocean prevails while the suppressed convection over the western Pacific tends to be weak and located south of the equator. Corresponding to this convective anomaly field, the upper tropospheric circulation is prominent in the Northern Hemisphere and features a circum-Pacific wavetrain emanating from South Asia to Mexico with three interim centers located at East Asia, extratropical North Pacific, and subtropical eastern North Pacific (Fig. 4a). At 850 hPa, the same wave train is hardly discernable; and the North Pacific is dominated by a gigantic anticyclonic anomaly (Fig. 4c). At Phase 7, the anomalous convection moves to the western Pacific while

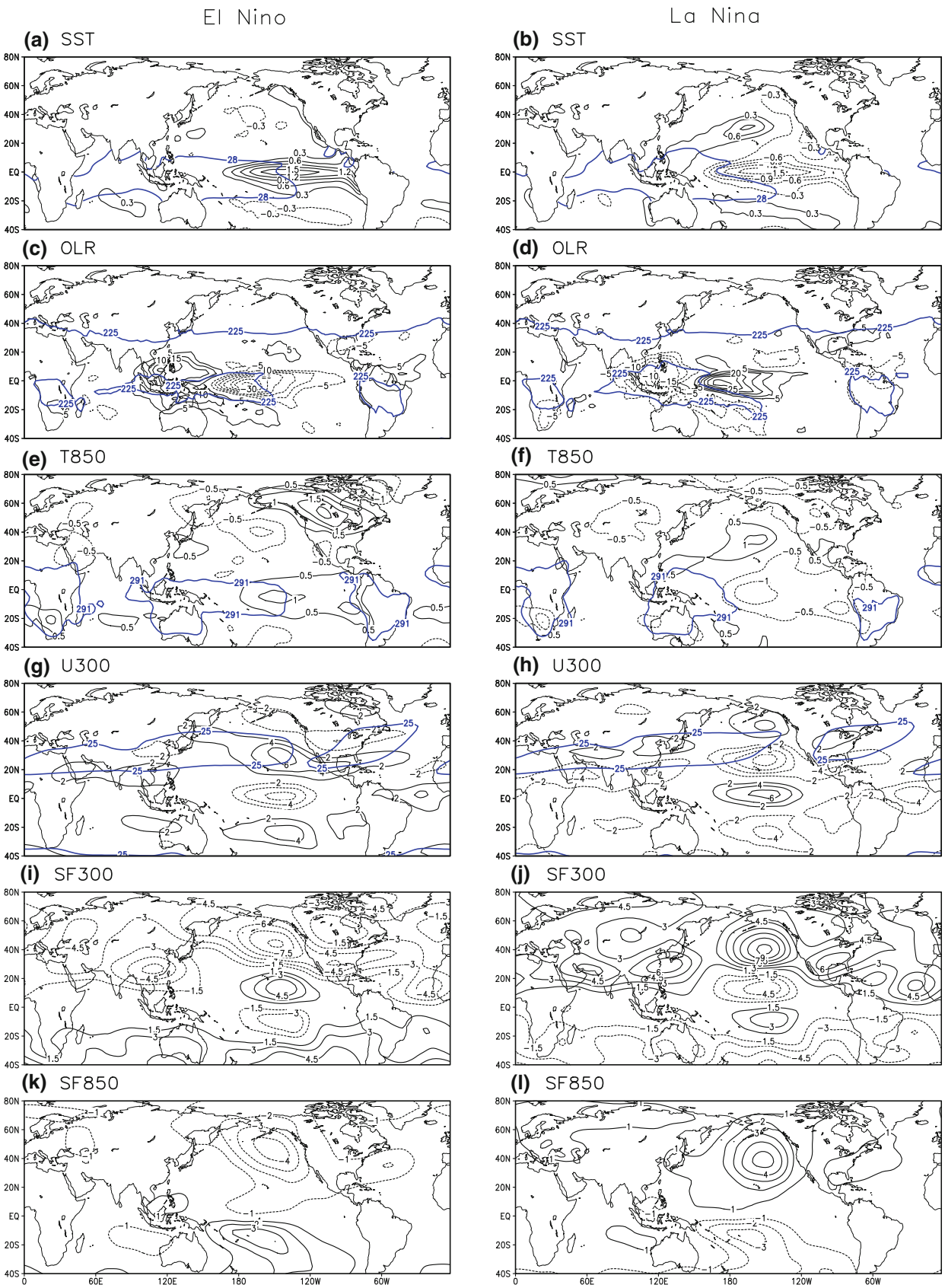
El Nino
La Nina
(a) SST
(b) SST
(c) OLR
(d) OLR
(e) T850
(f) T850
(g) U300
(h) U300
(i) SF300
(j) SF300
(k) SF850
(l) SF850
80N
60N
40N
20N
EQ
20S
40S
0
60E
120E
180
120W
60W

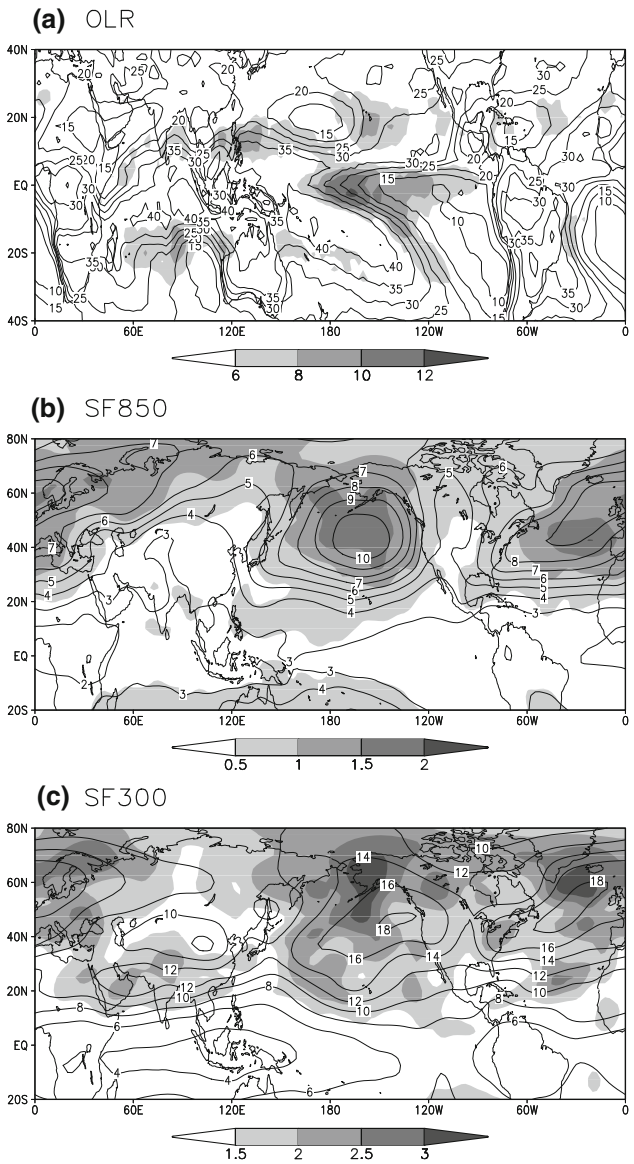

Fig. 2 Climatological winter (December–February) mean intraseasonal variability (ISV, contour) and interannual variation of ISV measured by the standard deviations of 29-year ISV anomalies (*shaded*) of **a** OLR, **b** 850 hPa streamfuntion (SF850), and **c** 300 hPa streamfunction (SF300). The unit of OLR is W/m^2 and the unit of streamfunction is 10^{-6} m/s

the eastern Indian Ocean is under control by strongly suppressed convection. The MJO convective anomaly pattern is almost the same as that in Phase 3 except with opposite polarities. As a result, both the upper and lower tropospheric rotation circulations are nearly a mirror image of those at Phase 3 except the anomalies over the Asian Pacific sector is weaker. The corresponding 850 hPa temperature anomalies are also tending flip over their signs between the Phase 3 and 7 (Fig. 4c, d). Different from Phase 3, at Phase 7 the circulation anomalies over the North America and North Atlantic are stronger in response to the convective anomaly that had moved to the western Pacific. The hemispheric asymmetric response of the rotational circulation is apparently due to the hemispheric asymmetry in the westerly jet between the Northern and Southern Hemisphere.

The result in Fig. 4 indicates that the joint tropical-extratropical intraseasonal variations have an action center in the North Pacific where the circulation anomalies tend to have opposite polarities between the MJO Phase 3 and Phase 7, and thereby the MJO paces extratropical intraseasonal pulsation. In order to facilitate careful comparison of the horizontal structures of MJO teleconnection between El Niño and La Niña years, the following two subsections along with Figs. 5 and 6 discuss contrasting features during these two most active phases of the MJO.

4.2 The MJO teleconnection in Phase 3 (Indian Ocean)

Figure 5 compares the composite OLR (color shading in the upper-panel), precipitable water (color shading in the lower-panel), 850 and 300 hPa circulations (streamfunction in contour, horizontal wind in vector), and 850 hPa temperature (thick contour in the lower-panel) at MJO Phase 3 (convection over the Indian Ocean) between El Niño and La Niña years. At the first glance, the two sets of composites seem to have similar tropical features in OLR (precipitable water) and the corresponding quadruple baroclinic circulation structure, namely, a pair of upper-level anticyclonic anomaly residing both sides of the convection over the Indian Ocean while a pair of cyclonic anomalies residing in both sides of the equatorial westerly anomalies over the western Pacific (Fig. 5a, b), a feature agrees well with the previous findings (Knutson and Weickmann 1987; Murakami 1988; Wang and Rui 1990). However, remarkable differences are observed in the tropics and especially in the extratropics. During La Niña years, the convection (negative OLR) anomaly over the Indian Ocean is stronger, larger, and more importantly, extended northward to southern India and Bay of Bengal than that of El Niño years. This is important because the corresponding convective heating-induced upper-level anticyclonic anomaly over the South Asia and the cyclonic anomaly over the tropical western North Pacific near the dateline are both substantially stronger during La Niña years than in El Niño years (Fig. 5a, b). As a result, the extratropical barotropic circulation patterns have pronounced differences between the El Niño and La Niña composites. First, over the East Asia and North Pacific, the extratropical response during La Niña years is obviously stronger than that during El Niño years. Second, during La Niña years, a huge anticyclonic circulation anomaly occupies nearly the entire North Pacific basin with a center located at (40°N, 180°E). This huge North Pacific

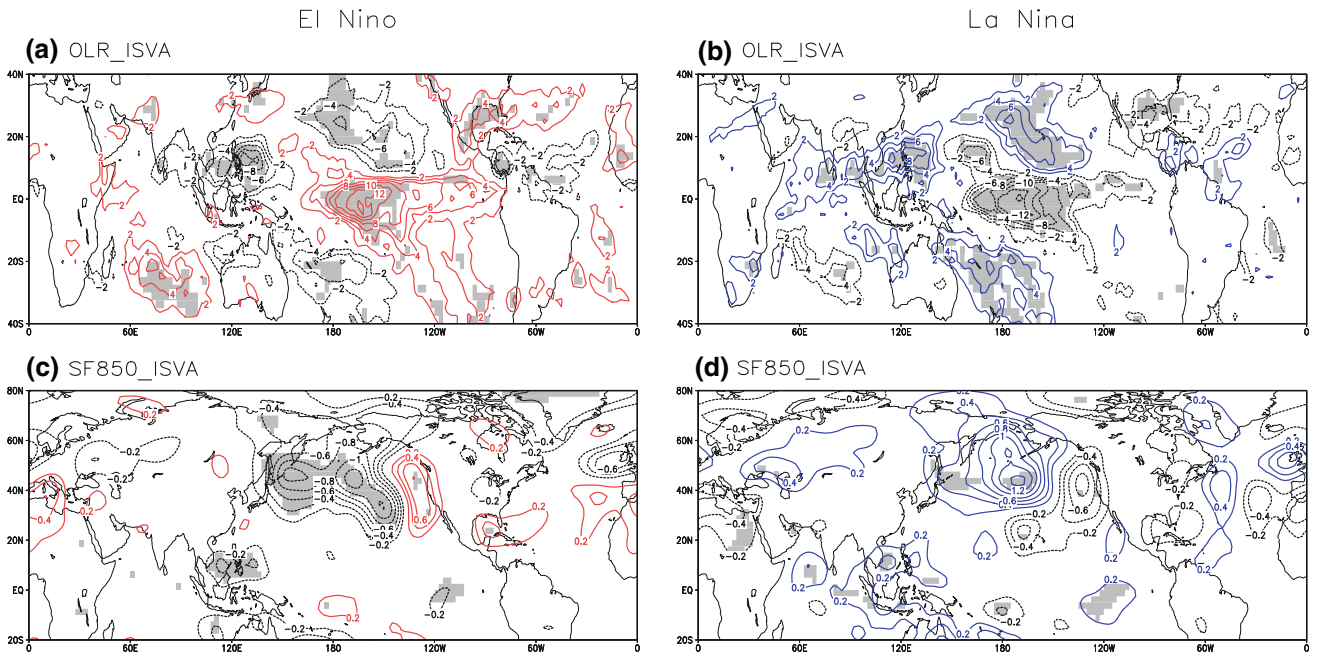

Fig. 3 The composite anomalies of the intraseasonal variability for **a**, **b** OLR, and **c**, **d** SF850. The *left panels* are for El Niño years and the *right panels* are for La Niña years. The *shaded regions* indicate that the differences between the ISVs during El Niño/La Niña and climatological ISV are statistically significant at above 90% confidence level by student's *t* test. Enhanced ISV anomaly is colored in *red* (*blue*) contour during El Niño (La Niña). The unit of OLR is W/m^2 and the unit of streamfunction is 10^{-6} m/s. The global patterns of OLR ISV anomalies in El Niño years are almost the same as La Niña years but with opposite polarities

anticyclonic anomaly advects cold air southward, causing colder than normal weather in the US west coast; meanwhile the warm advection makes a warmer than normal period over the east cost of East Asia. Large and enhanced moisture over the Indian Ocean in La Niña is transported along the coastline of Asian continent and western boundary of North Pacific High to northeastern East Asia (Fig. 5d). In sharp contrast, during El Niño years, the North Pacific anomalous anticyclone is much weaker, smaller in size, and shifting northward with a center at 50°N. This relatively small North Pacific anticyclonic anomaly can no longer affect US west coast and the east coast of East Asia, instead, the western US and Canada is under influence of warm advection associated with a low anomaly (Fig. 5c). Third, as a result of the change in the North Pacific anticyclonic anomaly, the corresponding Rossby wave train patterns downstream the North Pacific are very different: The eastern US is under influence of a cold dry cyclonic anomaly during El Niño years (Fig. 5c), whereas it is influenced by a warm anticyclonic anomaly during La Niña years (Fig. 5d); the North Atlantic is dominated by warm anticyclonic anomaly during El Niño years (Fig. 5c), whereas it is influenced by a cold cyclonic anomaly during La Niña years (Fig. 5d). In general, from the North America to Europe the high latitude circulation anomalies tend to have opposite signs between the El Niño and La Niña composite.

Figure 5a and b also indicate that the North Pacific anomaly is closely linked to the subtropical South Asian high and the subtropical low over the central North Pacific; they are associated with the enhanced convection over the Indian Ocean and suppressed convection over the equatorial western Pacific, respectively. The differences in extratropical teleconnection between La Niña and El Niño are in accordance with the differences of the MJO convective anomalies over the Indian Ocean and western North Pacific, reflecting the effects of ENSO modulation. Of note is that the MJO convection over the Indian Ocean at Phase 3 in La Niña has a stronger influence over the North Africa than during the El Niño years due to westward dispersion of upper level Rossby waves, which enhances upper level tropical easterly jet stream (Fig. 5b).

4.3 The MJO teleconnection in Phase 7 (western Pacific)

At Phase 7, the anomalous convection redevelops in the western Pacific after passing through the Maritime Continent. Similar to the conditions in Phase 3, the two sets of composites seem to have similar features in OLR (precipitable water) and the associated baroclinic circulation structure in the tropics (Fig. 6). However, the differences in the MJO convective activity and moisture distribution, such as the latitudinal and longitudinal locations between

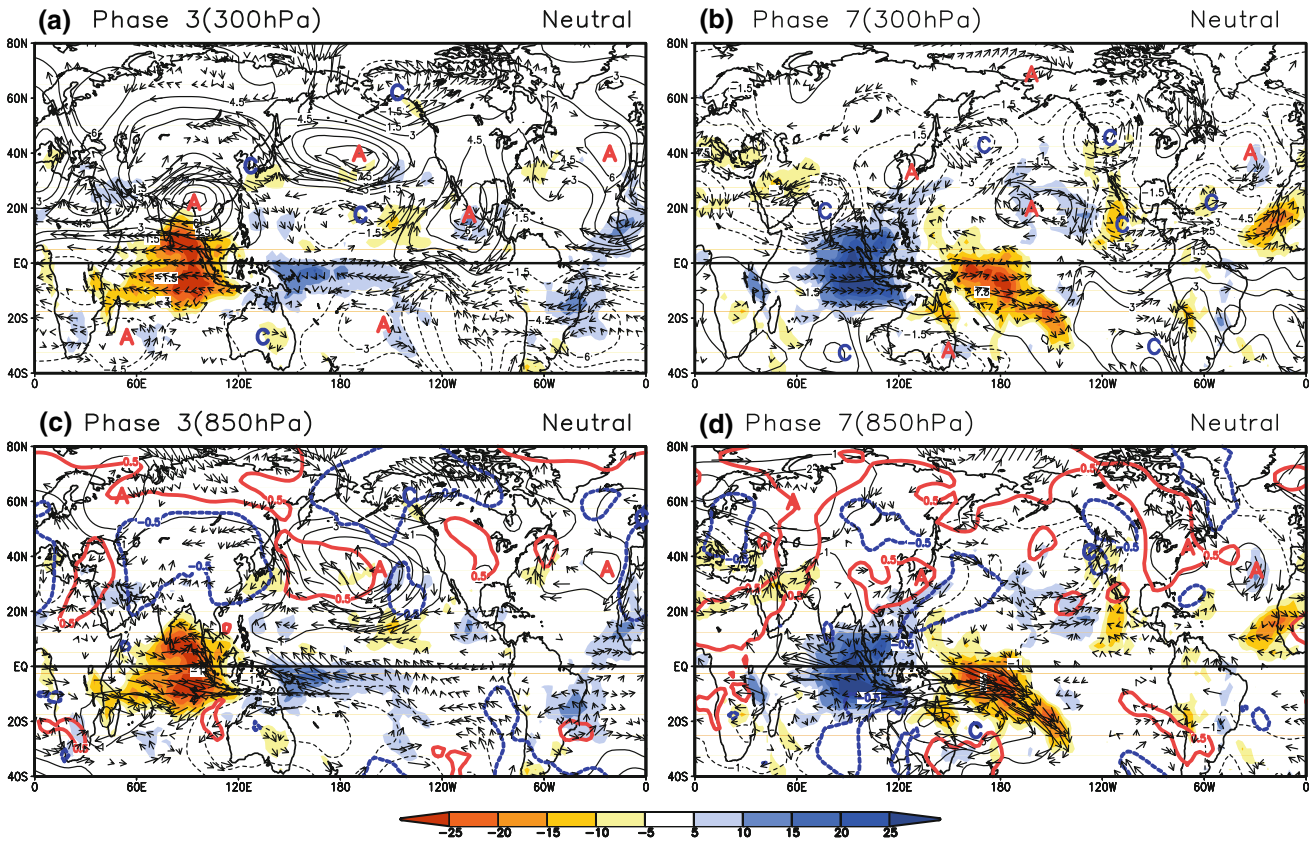

Fig. 4 Composite anomalies of **a**, **b** SF300 (contours) and winds (vectors) and **c**, **d** SF850 (contours) and winds during neutral years at Phase 3 (*left panel* when the convection is enhanced over the Indian Ocean) and at Phase 7 (*right panel* when the convection is enhanced over the western Pacific). OLR is *shaded* in (**a**)–(**d**). In (**c**) and (**d**), the *red* (*blue*) thick contours denote the 850 hPa temperature anomalies above (below) 0.5 (−0.5) °C. The units of OLR, streamfunction, and temperature are W/m^2, 10^{-6} ms^{-1}, and °C, respectively. Only the wind vectors that are statistically significant above 90% confidence level are plotted

El Niño and La Niña, are more noticeable than in Phase 3. This is expected because the MJO convection starts to decay at this stage and ENSO has stronger influences on the MJO propagation and development in the western Pacific than in the Indian Ocean. As seen from Fig. 6, during La Niña years the most prominent MJO convection over the western Pacific is located in the Philippine Sea, while during El Niño years it dramatically shifts southeastward to the central Pacific just south of the equator. The moisture field also shows similar structure. Corresponding to this drastic shift of convective anomaly, the most important feature in the tropical MJO circulation anomaly is the shift of the anomalous (upper level anticyclonic and cyclonic) circulation along 20°N from the Philippine Sea during La Niña to the central North Pacific during El Niño years. This shift has most profound impacts on the development of the extratropical response of the MJO teleconnection. In neutral year (Fig. 4b), the center of the anticyclonic flow to the north of the convection is located between that of La Niña (west) and El Niño (east). This indicates that the enhanced convection over the Philippine Sea during La Niña has induced westward shift of the anticyclonic flow to its north and also strengthened extratropical response (cyclonic flow) over the North Pacific.

Over the extratropical North Pacific, a barotropic cyclonic anomaly develops to the north of the subtropical anticyclonic anomaly in both the El Niño and La Niña composites. However, the cyclonic anomaly in La Niña years tends to be located in the western North Pacific (and elongated), whereas its counterpart during the El Niño shifts eastward and located primarily in the central-eastern North Pacific. As a result, during La Niña years, the western North Pacific cyclonic anomaly enhances the winter monsoon over northern Japan; whereas during El Niño years the central-eastern North Pacific cyclonic anomaly warms the west coast of US and Canada by advection of warm wet air from south. Furthermore, during the La Niña years, an evident great-circle like Rossby wave train is developed from the Philippine Sea to the eastern US (Fig. 6b). In contrast, during the El Niño years, the extratropical anomaly pattern shows an east–west oriented belt

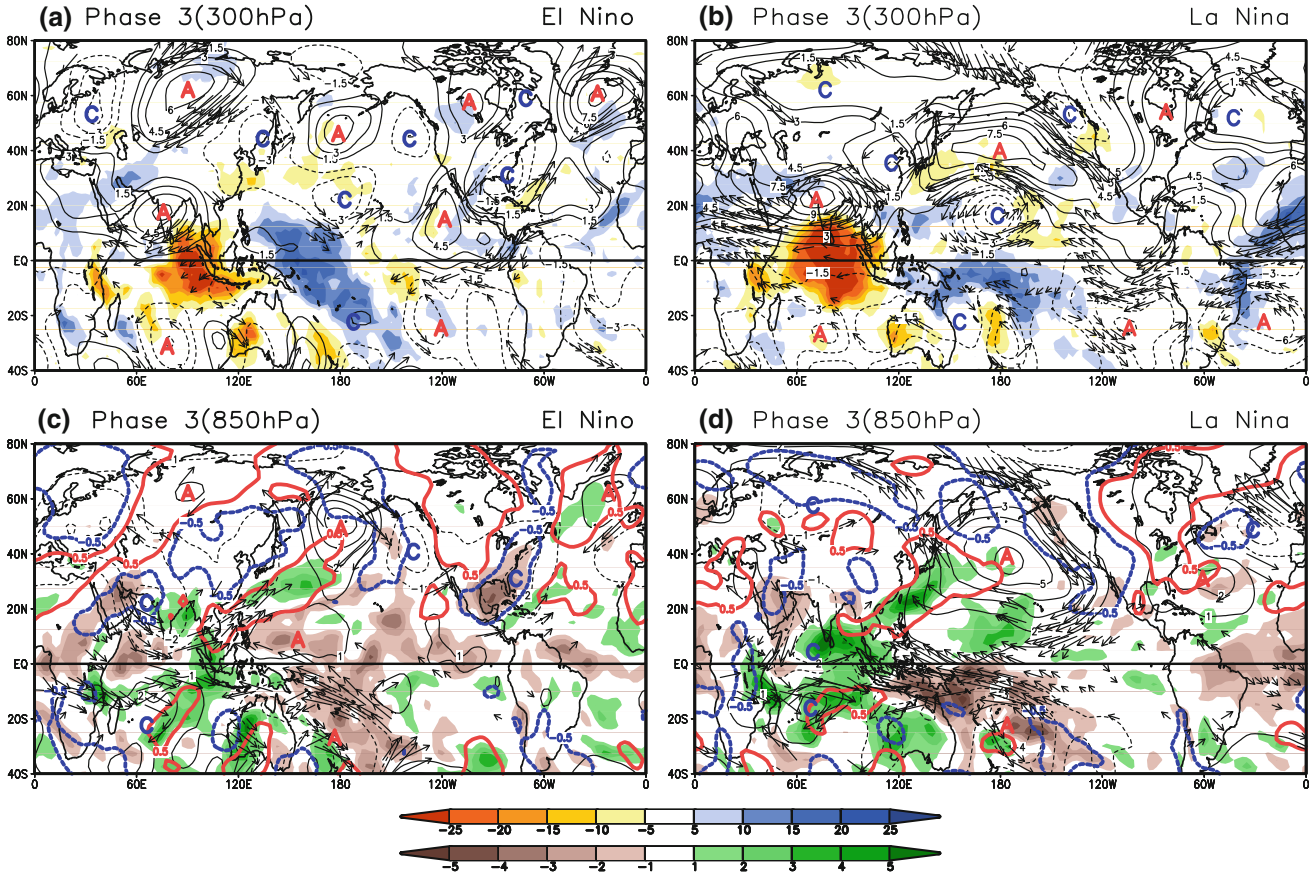

Fig. 5 Composite anomalies of **a**, **b** SF300 (contours) and winds and **c**, **d** SF850 (contours) and winds during El Niño (*left panel*) and La Niña years (*right panel*) at Phase 3 (when the convection is enhanced over the Indian Ocean). OLR and precipitable water during ENSO are *shaded* in **a**–**b** and **c**–**d**, respectively. In (**c**) and (**d**) and the *red* (*blue*) thick contours denote the 850 hPa temperature anomalies above (below) 0.5 (−0.5) °C. The units of OLR, precipitable water, streamfunction, and temperature are W/m^2, kg/m^2, 10^{-6} ms^{-1}, and °C, respectively. Only the wind vectors that are statistically significant above 90% confidence level are plotted

centered around 40°N with three centers at 160°W (low), 110°W (high), and 70°W (low) (Fig. 6a, c), which are coupled with the upper tropospheric, tropical anomaly centers with opposite signs to their south (Fig. 6a). The associated US temperature and moisture anomalies in the low level are just opposite as those during La Niña years, i.e., a dipole pattern consisting of a warm wet west pole versus a cold dry east pole. Hence, the MJO teleconnection over North America is highly dependent on the ENSO extreme phases.

The result here suggests that the anomalous MJO convection located in the off-equatorial western Pacific can modulate the strength and location (latitude and longitude) of the subtropical circulation anomalies in the North Pacific and the associated extratropical teleconnection patterns over North America. This result is consistent with the notion that the change of position in the anomalous tropical convection can induce a large difference over the extratropical flow (Branstator 2003) and the notion that the Pacific-North American sector is sensitive to the tropical Pacific SST (Hoering and Kumar 2002; Mori and Watanabe 2008).

Note that at Phase 7 when MJO convection anomaly moves to the western Pacific, the Indian Ocean is dominated by subsidence, while the West Africa is wet and North Atlantic Ocean tends to be significantly affected. However, during both El Niño and La Niña years, a similar barotropic circulation anomaly pattern tends to occur over North Atlantic, which favors a negative phase of the North Atlantic Oscillation (NAO; Fig. 6). This suggests that the MJO impact on North Atlantic at Phase 7 tends to be independent of ENSO phases. Interaction between the Madden–Julian Oscillation and NAO may make NAO predictable, to some extent, on subseasonal time scale (Cassou 2008).

We note that in the tropics, the equatorial wave adjustment to heating is rapid, taking about 4 days; while the extratropical response may take 2 weeks (Matthews et al. 2004). The composite pictures shown in Figs. 5 and 6 are snap shot portraits of the MJO teleconnection. Even

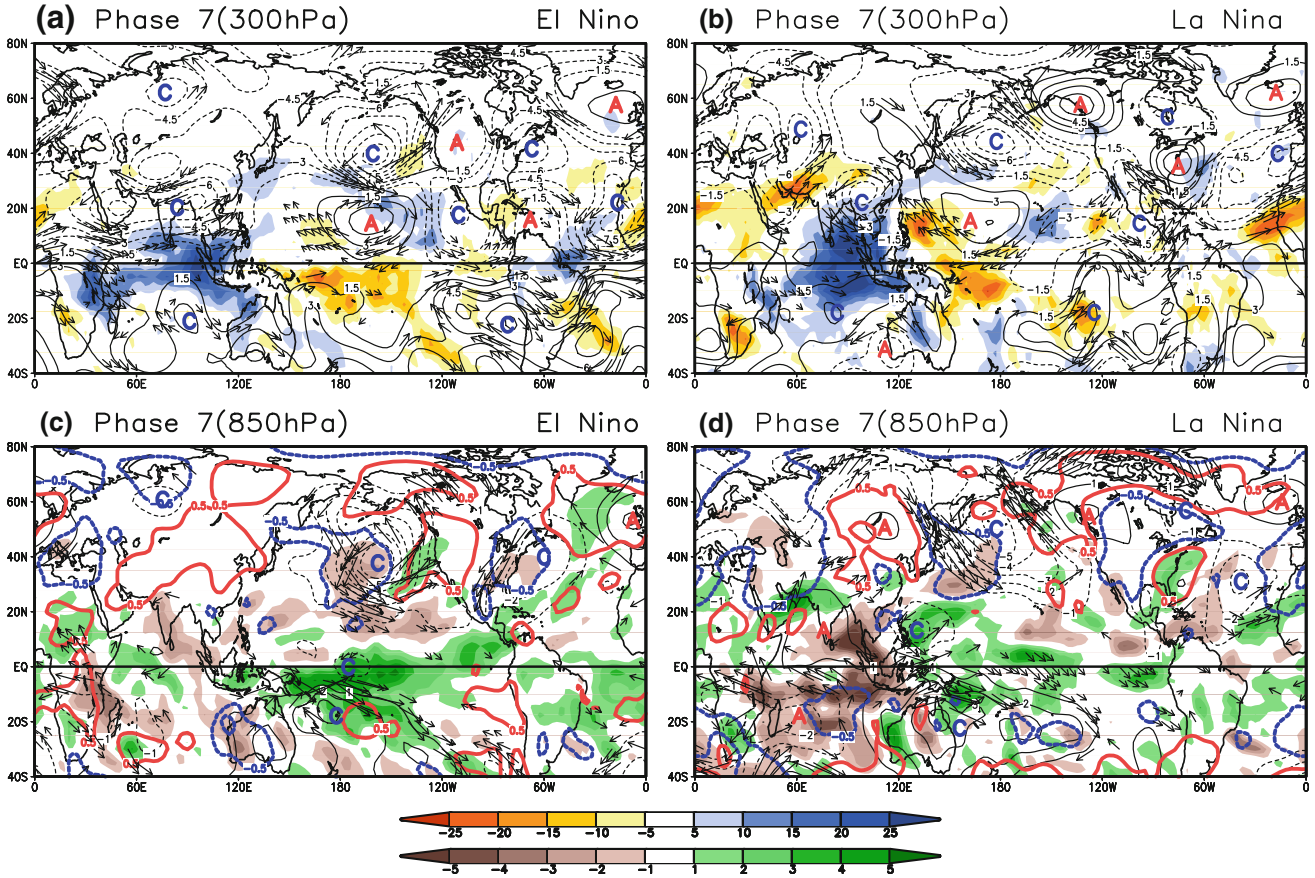

Fig. 6 Same as in Fig. 5, but for Phase 7 (when the convection is enhanced over the western Pacific)

though the MJO convective anomaly slowly propagates eastward, the associated tropical baroclinic quadruplet circulation anomaly can be viewed as an "instant" response; but over the extratropics, especially far away from the MJO heat sources the response may partially reflect the lagged impact of the MJO heating in the previous phase. Thus, it is interesting to further examine lead-lag MJO teleconnection.

Figure 7 shows the lead-lag MJO teleconnection maps at 300 hPa with respect to MJO at Phase 3. The composites of OLR and upper-level circulation from −5 day to +5 day are constructed when the convection is enhanced over the Indian Ocean. 0 day represents at MJO Phase 3 and −5 day (+5 day) depicts the intraseasonal anomalies that lead (lag) 5 days from Phase 3. It is seen that the extratropical wave trains associated with Indian Ocean active convection intensify with time in general, but the locations of the anomalous cells of the wave train from South Asia to North Atlantic tends to be steady in both the El Niño years (except over the North Atlantic) and La Niña years (except a northward shift of the cells over North America). The same conclusion holds for MJO Phase 7 (Figure not shown). These results suggest that the features seen in Figs. 5 and 6 are generally robust, even though they contain accumulative heating effect from the previous phases.

4.4 The MJO teleconnection with influence of ENSO

Note that the ENSO itself induces seasonal anomalies in the extratropics; it is needed to consider the respective strength of the interannual and intraseasonal anomalies. In Fig. 8, the composite maps are obtained by using the same method as shown in Sect. 4.2–4.3, but with the data without filtering out interannual variability (IAV); that is, the time mean and the first three harmonics of the annual cycle are first removed, then a 120-day mean during the previous 120 days is also subtracted; however, the interannual variability associated with ENSO are included.

The composite maps of MJO (OLR) and MJO teleconnection (SF300) at Phase 3 (upper-panel) and 7 (lower-panel) during El Niño and La Niña years show similar structures with those in Figs. 5 and 6. The difference of the OLR intraseasonal anomalies between the IAV-filtered (Figs. 5 and 6) and not filtered (Fig. 8) show a similar structure as the ENSO-induced seasonal anomalies shown

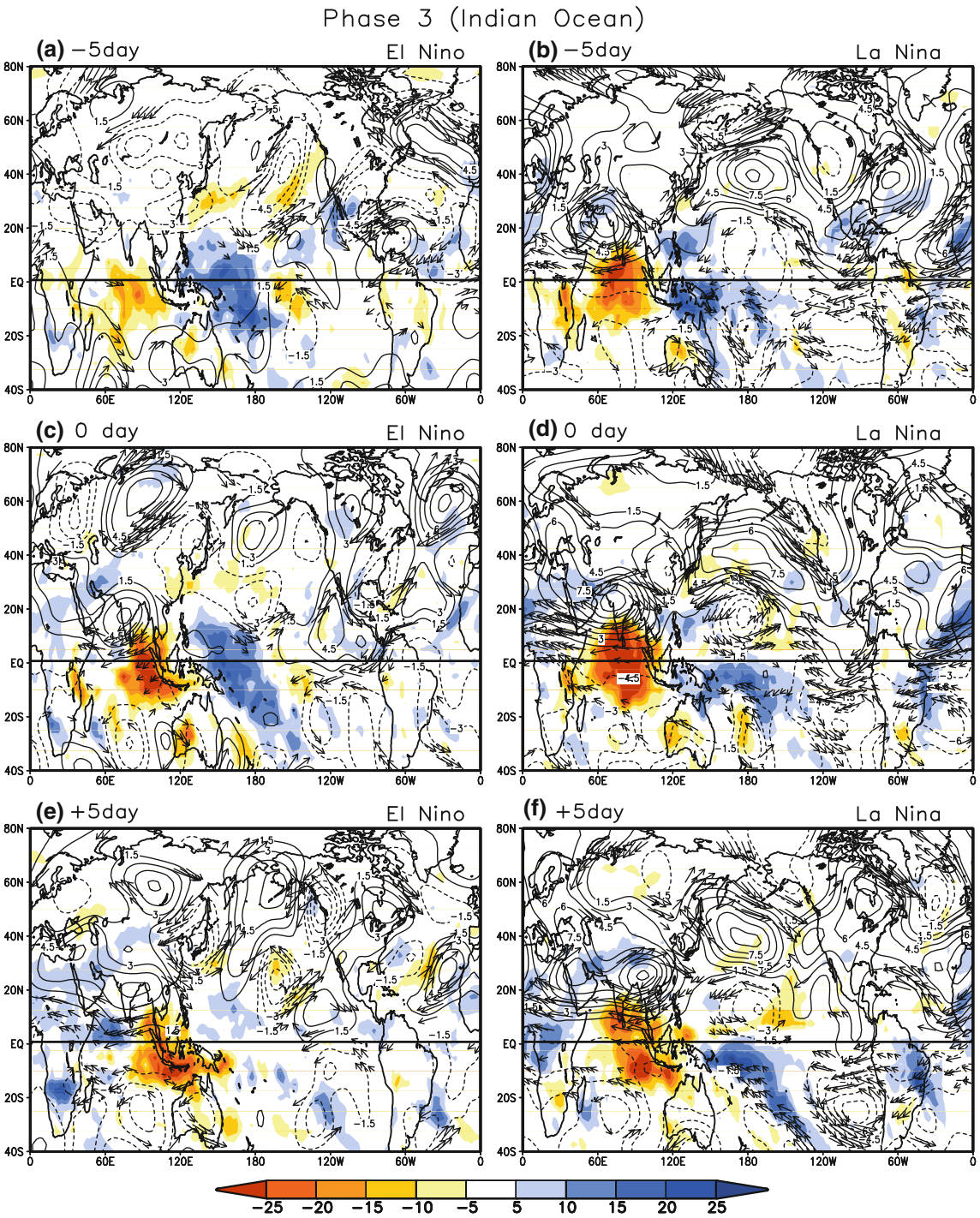

Fig. 7 Composite anomalies of SF300, OLR, and wind at 300 hPa during El Niño (*left panel*) and La Niña years (*right panel*) at **a**, **b** −5 day, **c**, **d** 0 day, and **e**, **f** +5 day when the convection is enhanced over the Indian Ocean (0 day represents at MJO Phase 3)

in Fig. 1c and d. The anomalies including IAV (total anomalies for short) are enhanced over the central-eastern Pacific near the equator at both Phase 3 and 7 in El Niño, but during La Niña the total anomalies are enhanced over the western Pacific with a meridional extension and in both sides of the equator over the central Pacific. The MJO teleconnection pattern and their maximum centers at each phase in the total anomalies have almost same locations with those obtained using filtered data. However, there exist intensity differences especially over the ENSO-teleconnection areas; that is, the South Asia, central-eastern Pacific through North America sectors. At Phase 3, the

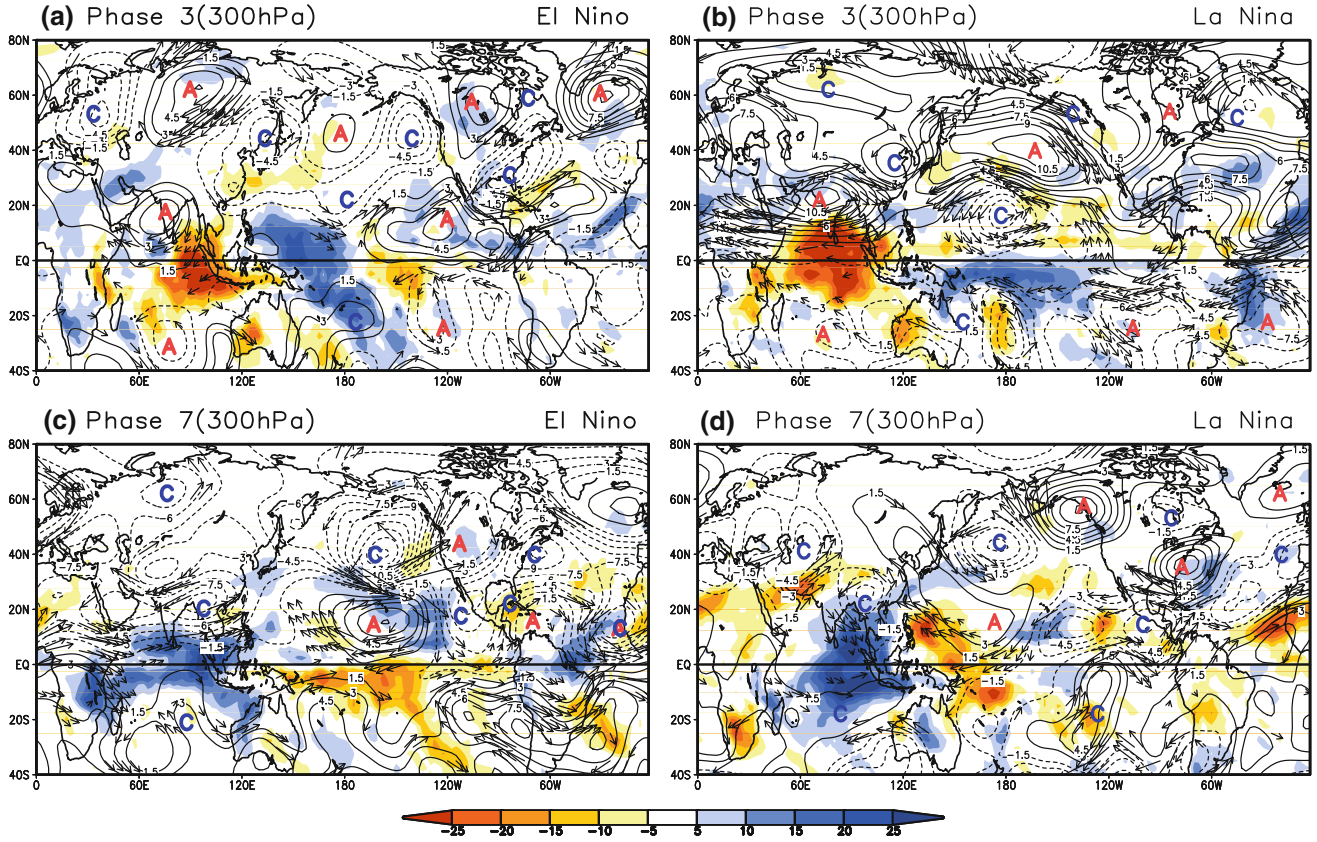

Fig. 8 Composite anomalies without filtering interannual variabilities of SF300 (contours) and winds (vectors) during El Niño (*left panel*) and La Niña years (*right panel*) at **a**, **b** Phase 3 and at **c**, **d** Phase 7. OLR is *shaded* in **a**–**d**. The units of OLR, streamfunction are W/m^2 and 10^{-6} ms^{-1}, respectively. Only the wind vectors that are statistically significant above 90% confidence level are plotted

anticyclonic anomalies over South Asia and North Pacific reduces its magnitude during El Niño but increases in La Niña; while the cyclonic anomaly at the western coast of Canada/subtropical central Pacific enhances/weakens during El Niño but the opposite occurs in La Niña. At Phase 7, the cyclonic/anticyclonic anomaly over the North Pacific is largely enhanced in El Niño but reduced during La Niña with the anticyclonic anomaly over the Canada much enhanced. The modulation of ISV anomaly by IAV is more evident at Phase 7 than Phase 3. The intensity changes of these centers follow the ENSO anomaly signals which were shown in Fig. 1i and j.

Comparing the result from Fig. 8 with Figs. 5 and 6 indicates that the intraseasonal anomalies at each phase of the MJO are affected by the ENSO anomalies, especially over the ENSO-teleconnection sectors. However, the phase-dependent MJO teleconnection shown in this study has significant and robust signals even in the presence of ENSO-induced seasonal anomalies. Hence, the "pure" MJO teleconnection can still be clearly identified with its action center over the North Pacific, which had opposite polarities between the MJO Phase 3 and Phase 7, although ENSO seasonal anomaly indeed modifies the teleconnection pattern.

5 Conclusion and discussion

The present study investigates interannual variations of the boreal winter MJO and its extratropical teleconnection in the Northern Hemisphere using observed data over the past 30 years (1979–2008). Large interannual variability of the MJO convection variance is found along the boundaries of the seasonal mean intraseasonal variability center; namely, along the latitude bands between 10° and 25° latitudes in both hemispheres over the Indian Ocean and western-central Pacific and at the equatorial central-eastern Pacific (Fig. 2a). The interannual variations of the ISV in 850 hPa rotational circulation exhibits strongest centers around 40°N over the North Pacific and North Atlantic, which coincides with its seasonal mean ISV centers (Fig. 2b). On the other hand, the large interannual variability of ISV in the upper-level circulation tends to be concentrated in two separate latitudinal bands, one at 20°–40°N and the other at

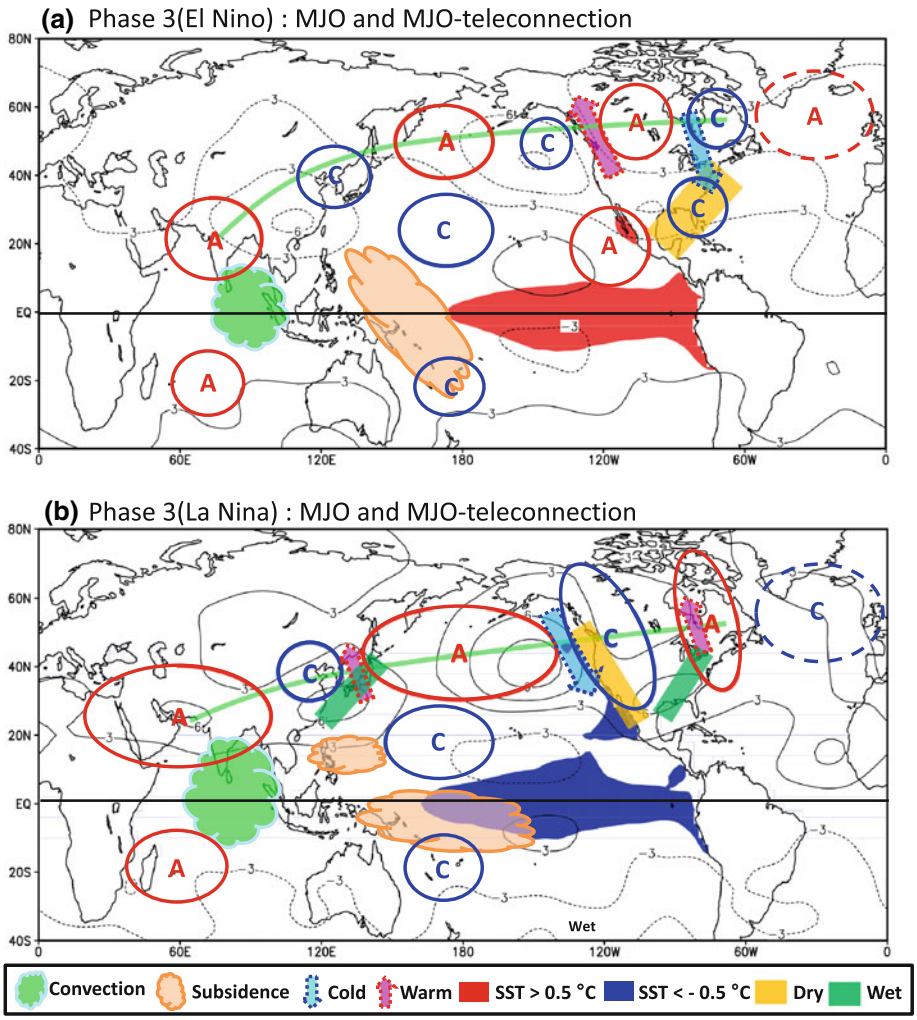

Fig. 9 The schematic diagrams illustrating the typical patterns of MJO-teleconnection at Phase 3 (convection enhanced over the Indian Ocean) during **a** El Niño and **b** La Niña years. *Black thin* contour displays composite anomalies of seasonal mean streamfunction at 300 hPa. *Blue* and *red thick* contours display MJO teleconnection at 300 hPa. Letter *A* (*C*) depicts anticyclonic (cyclonic) circulation anomaly. The winter mean SST anomaly during El Niño and La Niña is *shaded* in *red* ($T \geq 0.5°C$) and *blue* ($T \leq -0.5°C$), respectively. The *dotted blue* (*red*) *arrow* denotes cold (warm) advection. The *green* (*yellow*) rectangle denotes wet (dry) condition. Cloud shape in *green* represents convection associated with MJO and the cloud shape in *orange* denotes the subsidence at Phase 3. *Green thick line* indicates the succession path of cyclonic and anticyclonic anomalies departed from the convection

50°–70°N (Fig. 2c). We have demonstrated that the aforementioned interannual variability of MJO and its teleconnection are largely due to ENSO impacts.

How does ENSO affect intraseasonal variability in OLR and rotational circulation? During El Niño the ISV of OLR is enhanced over the equatorial central-eastern Pacific, while during La Niña it intensifies over the periphery of the Indo-Pacific warm pool and subtropical central Pacific, especially over the Philippine Sea (Fig. 3a, b). The contrast in the MJO heat source (implied by OLR) between the El Niño and La Niña is attributed to the changes in seasonal mean SST anomalies: Positive SST anomaly centers are located at the equatorial central Pacific in El Niño, but at the off-equatorial regions of the western Pacific in both hemispheres during La Niña (Fig. 1). The seasonal mean upper-level circulations change significantly in accord with the northward (southward) movement of the jet stream during La Niña (El Niño) over the Asia—North Pacific—North America. The corresponding rotational flows also show contrasting features between the El Niño and La Niña years. In the low-level, the enhanced (weakened) ISV is detected over the South China Sea and Philippine Sea in La Niña (El Niño) years (Fig. 3c, and d), which is related to the enhanced (suppressed) convection there during La Niña (El Niño) years.

How does ENSO regulate the MJO teleconnection patterns? The MJO teleconnection depends on its phase of propagation. The ENSO regulation on MJO teleconnection at two important phases is examined in which the active MJO convection is located over the Indian Ocean (Phase 3) and the western Pacific Ocean (Phase 7), respectively. Two schematic diagrams, Figs. 9 and 10, summarize our major findings, which were made based on the major results shown in Figs. 5 and 6, respectively. In addition, the seasonal mean anomalies of upper-level rotational wind associated with ENSO is plotted to show how they are related to MJO teleconnection. The tropical circulation anomalies between 20°S and 20°N are essentially baroclinic, while outside of the tropics are equivalent barotropic. The schematic diagram highlights major rotational circulation systems at 300 hPa with reference to those at the 850 hPa. Since the common structure of the MJO

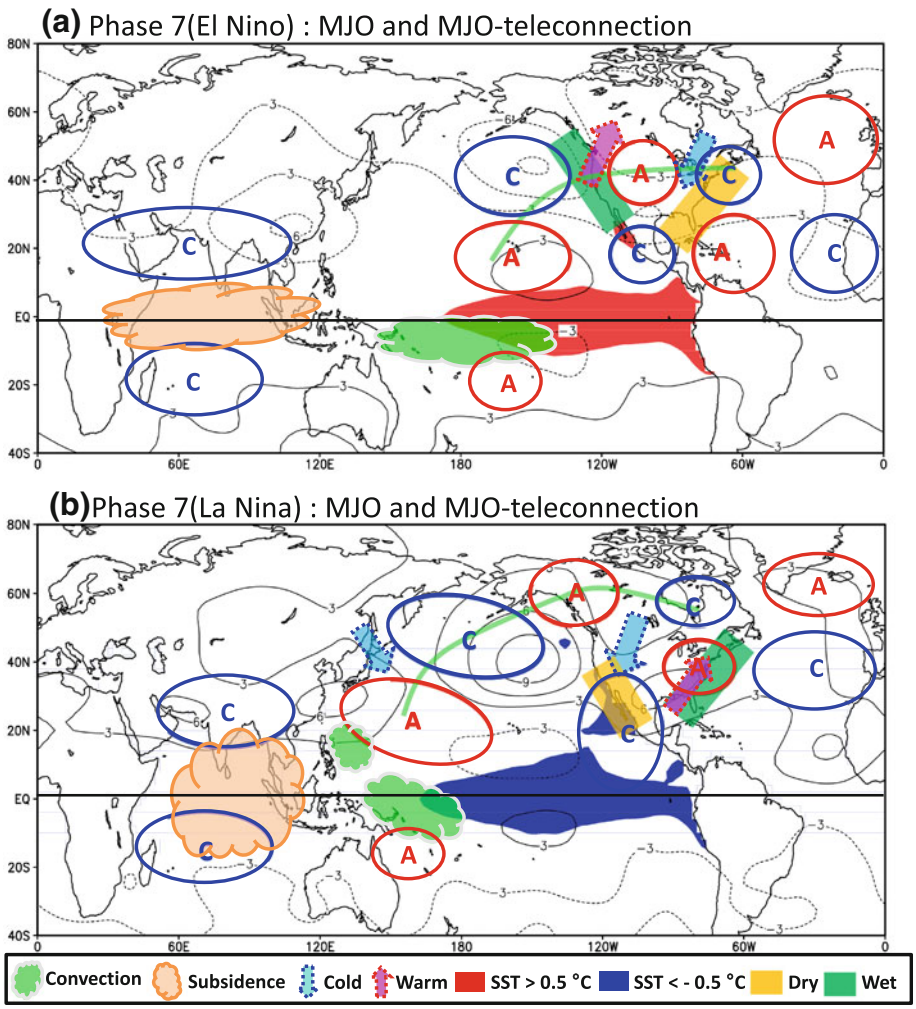

Fig. 10 Same as in Fig. 9, except for the case at MJO Phase 7 (convection enhanced over the western Pacific)

between El Niño and La Niña has been discussed in Sect. 4, the summary here focuses on the differences in MJO teleconnection between El Niño and La Niña years.

When the MJO convection develops and matures over the Indian Ocean (Figs. 5 and 9), we found that both the MJO in the tropics and MJO teleconnection in the extratropics exhibit pronounced differences between opposite phases of ENSO. During La Niña years, the Indian Ocean convection is much stronger, larger in size, and extends more northward than during El Niño years. As a result, the corresponding upper-level anomalous South Asian anticyclone and Philippine Sea cyclone are stronger than those during the El Niño years, so are the extratropical anomalies over East Asia and North Pacific. During La Niña, a gigantic anticyclonic anomaly occupies the entire North Pacific, causing warmer and wetter than normal weather over the northeast coast of East Asia through northward warm advection and colder and drier weather in the US west coast by cold advection. Further downstream, the Rossby wave train induces warm air advection to the eastern US. During El Niño, on the other hand, the North Pacific anticyclonic anomaly is relatively small and cannot affect US west coast, hence the US northwest coast is under influence of a low anomaly and warm advection, while the eastern US is affected by cold advection and dry conditions. At Phase 3 of MJO, the teleconnection pattern over the subtropics to extratropics of the North Pacific will be counterbalanced by seasonal mean anomaly (anticyclonic in the subtropics, cyclonic to the north) in El Niño but will be enhanced by the seasonal anomaly (cyclonic in the subtropics, anticyclonic to the north) during La Niña.

As the convection moves to the western Pacific (Figs. 6, 10), the differences in MJO convective activity between El Niño and La Niña are more salient than when the MJO convection is at the Indian Ocean. The enhanced MJO convection is located over the Philippine Sea in La Niña years, while it shifts to the central Pacific south of the equator in El Niño years. Corresponding to these remarkably different anomalous convective activities, the upper-level anticyclonic circulation anomaly forms over the Philippine Sea in La Niña but over the subtropical central North Pacific (near Hawaii) in El Niño. This movement of

the anticyclonic flow is consistent with the ENSO-teleconnection pattern in which the anticyclonic flow is more enhanced over the South China Sea (eastern Pacific) during La Niña. As a result, the corresponding extratropical cyclonic anomaly tends to locate in the western North Pacific in La Niña years, causing bitter winter monsoon over Japan; whereas during El Niño years it is located in the eastern-central North Pacific, warming the west coast of US and Canada. The temperature anomaly distribution over the US forms a dipole, that is, warm west and cold east in El Niño with opposite polarities in La Niña years. The moisture anomaly also shows opposite distribution between El Niño and La Niña. Further, during El Niño, the northeastern Pacific has a barotropic seasonal mean cyclonic anomaly, which will be enhanced by the MJO teleconnection when the MJO convective anomaly is located over the western Pacific (Phase 7). In contrast, during La Niña, the northeastern Pacific has a barotropic seasonal mean anticyclonic anomaly, which will be offset by the MJO teleconnection pattern. This indicates that when the MJO convective anomalies move to western Pacific, its associated extratropical anomalies in the northeastern Pacific will be enhanced during El Niño but reduced during La Niña; thereby the impacts of MJO teleconnection at Phase 7 on the North America is expected to be stronger during El Niño than during La Niña.

The results shown in Figs. 9 and 10 confirm that the extratropical North Pacific is an action center for MJO teleconnection, which determines its impacts on East Asia and North American weather conditions. This is true regardless of the MJO phases. Second, the extratropical North Pacific circulation anomalies have opposite polarity between MJO Phase 3 (when convection is active over the Indian ocean) and Phase 7 (when the convection is active over the western Pacific), indicating that the extratropical intraseasonal pulsation is paced by eastward propagation of MJO. Third, the MJO teleconnection is generally stronger during La Niña than during El Niño years. Fourth and most importantly, even in the same MJO phase, the North Pacific anomaly may differ remarkably between the extreme phases of ENSO so that the MJO impacts on East Asia and North America tend to be opposite between El Niño and La Niña years. This implies that making a composite MJO teleconnection without distinguishing ENSO phases may be fruitless due to smearing the effect of ENSO regulation. Hence, prediction of MJO impacts on North Pacific and adjacent East Asia and North America must take into account the ENSO regulation. Schematic diagrams Figs. 9 and 10 provide guidance for such predictions.

Note that the robust MJO teleconnection pattern at Phase 3 is confined to North America; while at Phase 7 when active convection is located over the western Pacific; its robust signal may reach North Atlantic and West Africa. Further, when MJO convective anomaly moves to the western Pacific, the Indian Ocean is dominated by subsidence; meanwhile the West Africa has increased rainfall and North Atlantic Ocean features an anomaly blocking pattern that favors a negative phase of the North Atlantic Oscillation (NAO; Fig. 6). This suggests that the MJO impacts on West Africa and North Atlantic at Phase 7 tend to be independent of ENSO phases. Hence, composite MJO teleconnection signal over the Atlantic-African sector should be strong even without distinguishing ENSO phases.

As has been shown by Matthews et al. (2004), the extratropical response to MJO-like heating is consistent with the theories of Rossby wave forcing and dispersion on the seasonal mean flow. ENSO may influence MJO teleconnection through a number of mechanisms. First, ENSO can affect the strength and location of the MJO convective anomalies at various phases of its propagation through modifying tropical mean circulation as shown in Figs. 3, 5, 6. The change of MJO convection on interannual time scale holds a key for understanding of the interannual variation of the MJO teleconnection. Second, ENSO can also change the subtropical and extratropical seasonal mean circulations, such as the jet stream. Change in the mean circulation may not only modify the distribution and strength of the Rossby wave forcing (Sardeshmukh and Hoskins 1987) and dispersion (Hoskins and Karoly 1981), but also the barotropic instability of the basic state that could partially determine extratropical teleconnection patterns (Simmons et al. 1983). However, the relatively roles of the changes in MJO convection position/intensity and the changes in the mean circulation in accounting for the differences between El Niño and La Niña remains elusive. Further model studies are underway to address this issue. Further studies are also underway to investigate ENSO regulation of MJO teleconnection in Southern Hemisphere and ENSO regulation of intraseasonal variability during boreal summer.

Acknowledgments This work was funded by the Climate Dynamics Program of the National Science Foundation under award No ATM-0647995, Korea Meteorological Administration Research and Development Program under Grant CATER 2009-1146, and the Korean Ministry of Environment as "The Eco-technopia 21 project". This manuscript is SOEST contribution No. 8003 and IPRC contribution No. 715.

References

Bergman JW, Hendon HH, Weickmann KM (2001) Intraseasonal air-sea interaction at the onset of El Niño. J Clim 14:1702–1719

Branstator G (2003) Remote response to tropical heating via the subtropical jet waveguide. 4th conference on atmospheric and oceanic fluid dynamics, 9–13 June 2003, San Antonio, Texas

Cassou C (2008) Intraseasonal interaction between the Madden–Julian oscillation and the North Atlantic oscillation. Nature 455:523–527

Chen WY, Van den Dool HM (1997) Asymmetric impact of tropical SST anomalies on atmospheric internal variability over the North Pacific. J Atmos Sci 54:725–740

Compo GP, Sardeshmukh PD, Penland C (2001) Changes of subseasonal variability associated with El Niño. J Clim 14:3356–3374

Drosdowsky W, Chambers LW (2001) Near-global sea surface temperature anomalies as predictors of Australian seasonal rainfall. J Clim 14:1677–1687

Ferranti L, Palmer TN, Molteni F, Klinker E (1990) Tropical-extratropical interaction associated with the 30–60 day oscillation and its impact on medium and extended range prediction. J Atmos Sci 47:2177–2199

Fink A, Speth P (1997) Some potential forcing mechanisms of the year-to-year variability of the tropical convection and its intraseasonal (25–70 day) variability. Int J Climatol 17:1513–1534

Hendon HH, Salby ML (1994) The life cycle of the Madden–Julian oscillation. J Atmos Sci 51:2225–2237

Hendon HH, Zhang C, Glick JD (1999) Interannual variation of the Madden–Julian oscillation during austral summer. J Clim 12:2538–2550

Hendon HH, Wheeler MC, Zhang C (2007) Seasonal dependence of the MJO-ENSO relationship. J Clim 20:531–543

Higgins RW, Mo KC (1997) Persistent north Pacific circulation anomalies and the tropical intraseasonal oscillation. J Clim 10:223–244

Higgins RW, Schemm JKE, Shi W, Leetmaa A (2000) Extreme precipitation events in the western United States related to tropical forcing. J Clim 13:793–820

Hoering MP, Kumar A (2002) Atmospheric response patterns associated with tropical forcing. J Clim 15:2184–2203

Hoskins BJ, Karoly D (1981) The steady linear response of a spherical atmosphere to thermal and orographic forcing. J Atmos Sci 38:179–196

Hsu HH (1996) Global view of the intraseasonal oscillation during northern winter. J Clim 9:2386–2406

Kalnay E et al (1996) The NCEP/NCAR 40-Year Reanalysis Project. Bull Amer Meteor Soc 77:437–471

Kemball-Cook S, Wang B, Fu X (2002) Simulation of the intraseasonal oscillation in the ECHAM-4 model: the impact of coupling with an ocean model. J Atmos Sci 59:1433–1453

Kessler WS (2001) EOF representation of the Madden–Julian oscillation and its connection with ENSO. J Clim 14:3055–3061

Kessler WS, Kleeman R (2000) Rectification of the Madden–Julian Oscillation into the ENSO cycle. J Clim 13:3560–3575

Kiladis GN, Straub KH, Haertel PT (2005) Zonal and vertical structure of the Madden–Julian oscillation. J Atmos Sci 62:2790–2809

Kim BM, Lim GH, Kim KY (2006) A new look at the midlatitude-MJO teleconnection in the northern hemisphere winter. Q J R Meteor Soc 132:485–503

Knutson TR, Weickmann KM (1987) 30–60 day atmospheric oscillations: composite life cycles of convection and circulation anomalies. Mon Wea Rev 115:1407–1436

Knutson TR, Weickmann KM, Kutzbach JE (1986) Global-scale intraseasonal oscillations of outgoing longwave radiation and 250 mb zonal wind during northern hemisphere summer. Mon Wea Rev 114:605–623

Lau KM (2005) El Niño Southern oscillation connection. In: Lau WKM, Waliser DE (eds) Intraseasonal variability in the atmosphere-ocean climate system. Praxis Publishing, UK, pp 271–300

Lau KM, Chan PH (1988) Intraseasonal and interannual variations of tropical convection: A possible link between 40–50 day oscillation and ENSO? J Atmos Sci 45:506–521

Lau KM, Philips TJ (1986) Coherent fluctuations of extratropical geopotential height and tropical convection in intraseasonal time scales. J Atmos Sci 43:1164–1181

Lau KM, Shen S (1988) On the dynamics of intraseasonal oscillations and ENSO. J Atmos Sci 45:1781–1797

Lorenc AC (1984) The evolution of planetary-scale 200 mb divergences during the FGGE year. Q J R Meteor Soc 110:427–441

Madden RA, Julian PR (1971) Detection of a 40–50 day oscillation in the zonal wind in the tropical Pacific. J Atmos Sci 28:702–708

Madden RA, Julian PR (1994) Observation of the 40–50 day tropical oscillation—a review. Mon Wea Rev 122:814–837

Matthews AJ (2000) Propagation mechanisms for the Madden–Julian oscillation. Q J R Meteor Soc 126:2637–2652

Matthews AJ, Hoskins BJ, Masutani M (2004) The global response to tropical heating in the Madden–Julian oscillation during northern winter. Q J R Meteor Soc 130:1991–2012

Mori M, Watanabe M (2008) The growth and triggering mechanism of the PNA: a MJO-PNA coherence. J Meteor Soc Jpn 86:213–236

Murakami T (1988) Intraseasonal atmospheric teleconnection patterns during the northern hemisphere winter. J Clim 1:117–131

Namias J (1986) Persistence of flow patterns over North America and adjacent ocean sectors. Mon Wea Rev 114:1368–1383

Pohl B, Matthews AJ (2007) Observed changes in the lifetime and amplitude of the Madden–Julian oscillation associated with the interannual ENSO sea surface temperature anomalies. J Clim 20:2659–2674

Rui H, Wang B (1990) Development characteristics and dynamic structure of tropical intraseasonal convection anomalies. J Atmos Sci 47:357–379

Sardeshmukh PD, Hoskins BJ (1987) On the derivation of the divergent flow from the rotational flow: the chi-problem. Q J R Meteor Soc 113:339–360

Simmons AJ, Wallace JM, Branstator GW (1983) Barotropic wave propagation and instability, and atmospheric teleconnection patterns. J Atmos Sci 40:1363–1392

Slingo JM, Rowell DP, Sperber KR, Nortley F (1999) On the predictability of the interannual behaviour of the MadMadden–Julian oscillation and its relationship with El Niño. Q J R Meteor Soc 125:583–609

Sperber KR (2003) Propagation and the vertical structure of the Madden–Julian oscillation. Mon Wea Rev 131:3018–3037

Takayabu YN, Iguchi T, Kachi M, Shibata A, Kanzawa H (1999) Abrupt termination of the 1997–98 El Niño in response to a Madden–Julian oscillation. Nature 402:279–282

Tam CY, Lau NC (2005) The impact of ENSO on atmospheric intraseasonal variability as interred from observations and GCM simulations. J Clim 18:1902–1924

Teng H, Wang B (2003) Interannual variations of the boreal summer intraseasonal oscillation in the Asia-Pacific region. J Clim 16:3572–3584

Trenberth KE (1997) The definition of El Niño. Bull Amer Meteor Soc 78:2771–2777

Waliser D et al (2009) MJO simulation diagnostics. J Clim 22:3006–3030

Wallace JM, Gutzler DS (1981) Teleconnections in the geopotential height field during the northern hemisphere winter. Mon Wea Rev 109:784–812

Wang B, Rui H (1990) Synoptic climatology of transient tropical intraseasonal convection anomalies: 1975–1985. Meteor Atmos Phys 44:43–61

Weickmann KM (1991) El Niño Southern oscillation and the Madden–Julian (30–60 day) oscillation during 1981–1982. J Geophys Res 96:3187–3196

Wheeler MC, Hendon HH (2004) An all season real-time multivariate MJO index: development of an index for monitoring and prediction. Mon Wea Rev 132:1917–1932

Yun KS, Seo KH, Ha KJ (2008) Relationship between ENSO and northward propagating intraseasonal oscillation in the east Asian summer monsoon system. J Geophys Res 113:D14120. doi: 10.1029/2008JD009901

Yun KS, Ren B, Ha KJ, Chan JCL, Jhun JG (2009) The 30–60 day oscillation in the East Asian summer monsoon and its time-dependent association with the ENSO. Tellus 61A:565–578

Zhang C, Gottschalck J (2002) SST anomalies of ENSO and the Madden–Julian oscillation in the equatorial Pacific. J Clim 15:2429–2445